J. Biochem. 132, 759–765 (2002)

Structure of Imidazole Glycerol Phosphate Synthase from *Thermus thermophilus* HB8: Open-Closed Conformational Change and Ammonia Tunneling[1]

Rie Omi,[*,†] Hiroyuki Mizuguchi,[‡] Masaru Goto,[*,†] Ikuko Miyahara,[*,†] Hideyuki Hayashi,[‡] Hiroyuki Kagamiyama,[‡] and Ken Hirotsu[*,†,2]

[*]Department of Chemistry, Graduate School of Science, Osaka City University, Sugimoto, Sumiyoshi-ku, Osaka 558-8585; [†]Harima Institute / SPring-8, The Institute of Physical and Chemical Research (RIKEN), Sayo-gun, Hyogo 679-5148; and [‡]Department of Biochemistry, Osaka Medical College, Takatsuki, Osaka 569-8686

Received July 24, 2002; accepted August 27, 2002

Imidazole glycerol phosphate synthase (IGPs) catalyzes the fifth step in the histidine biosynthetic pathway located at the branch point to *de novo* purine biosynthesis. IGPs is a multienzyme comprising glutaminase and synthase subunits. The glutaminase activity, which hydrolyzes glutamine to give ammonia, is coupled with substrate binding to the synthase subunit. The three-dimensional structure of the IGPs from *Thermus thermophilus* HB8 has been determined at 2.3 Å resolution, and compared with the previously determined structures for the yeast and *Thermotoga maritima* enzymes. The structure of each subunit is similar to that of the corresponding domain in the yeast enzyme or subunit in the *T. maritima* enzyme. However, the overall structure is significantly different from the yeast and *T. maritima* enzymes, indicating that IGPs may change the relative orientation between the two subunits and close the glutaminase site upon glutamine binding. The putative ammonia tunnel, which carries nascent ammonia from glutaminase to the synthase site, has a closed gate comprising a cyclic salt bridge formed by four charged residues of the synthase subunit. The side chain of Lys100 in the cyclic salt bridge might change its side chain direction to form new interactions with the main chain carbonyl group of glutamine from the synthase subunit and the hydoxyl group of tyrosine from the glutaminase subunit, resulting in the opening of the gate for ammonia transfer.

Key words: ammonia tunnel, conformational change, glutamine amidotransferase, imidazole glycerol phosphate synthase, three-dimensional structure, X-ray crystallography.

Glutamine-dependent amidotransferases hydrolyze the amide bond of glutamine to ammonia and glutamate, and transfer the nascent ammonia to an acceptor substrate to give an aminated product (*1–3*). Imidazole glycerol phosphate synthase (IGPs) is a member of a family of class I glutamine-dependent amidotransferases comprising two domains: glutaminase domains, which all evolved from the same ancestor, and synthase domains, which are evolutionally unrelated and have different functions in each enzyme. Recent X-ray studies on class I glutamine-dependent amidotransferases have shown that the ammonia produced in the glutaminase subunit is transferred to the synthase subunit through a channel formed inside the protein molecule (*4–9*), similar to the molecular tunnel observed in the structure of tryptophan synthase (*10–12*). IGPs catalyzes the hydrolysis of glutamine at the glutaminase subunit, and the reaction of nascent ammonia with N^1-[(5′-phosphoribulosyl)formimino]-5-aminoimidazole-4-carboxamide ribonucleotide (PRFAR) to produce imidazole glycerol phosphate (IGP) and 5-aminoimidazole-4-carboxamido-ribotide (AICAR) at the synthase subunit (Scheme 1) (*13*).

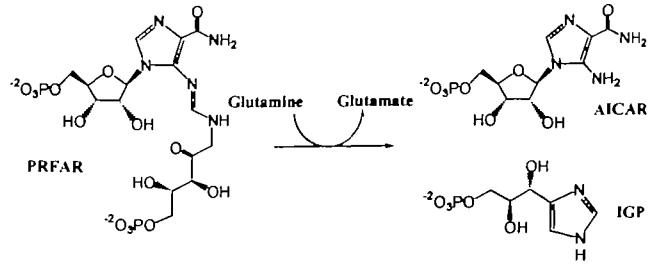

Scheme 1

Yeast IGPs consists of glutaminase and synthase domains on a single polypeptide chain (*14*). In bacteria, IGPs

[1] This study was supported in part by the following grants: Grant-in-Aid for Scientific Research on Priority Areas from the Ministry of Education, Science, Sports, and Culture of Japan [Category B: 13125207 (K.H.)], and Research Grant from the Japan Society for the Promotion of Science [Category B:13480196(K.H.)]. Coordinates for imidazole glycerol phosphate synthase have been deposited in the RSCB Protein Data Bank as entry 1KA9.

[2] To whom correspondence should be addressed. Fax: +81-6-6605-3131, E-mail: hirotsu@sci.osaka-cu.ac.jp.

Abbreviations: *tt*IGPs, yIGPs and *tm*IGPs, imidazole glycerol phosphate synthases from *Thermus thermophilus* HB8, yeast and *Thermotoga maritima*, respectively; Met1s and Met1g, Met1 residues from the synthase and glutaminase subunits, respectively; rms, root mean square.

is a multienzyme that is a product of the *hisF* and *hisH* genes of the histidine operon associated with the histidine and purine biosynthetic pathways. One subunit encoded by the *hisH* gene has the glutaminase activity, and the other subunit encoded by the *hisF* gene has the synthase activity. IGPs shows a strong glutaminase activity with the coupled glutaminase and synthase reaction in the presence of PRFAR, although a very weak activity is observed in the absence of PRFAR (*15, 16*). This implies that the binding of PRFAR to the synthase subunit induces a conformational change in the glutaminase subunit of IGPs to reorganize the glutamine binding region of the glutaminase subunit.

The X-ray structure of the isolated synthase subunit from *Thermotoga maritima* shows that the subunit has a $(\beta/\alpha)_8$ barrel fold (*17*). Quite recently, the structures of IGPs from yeast and *T. maritima* have been solved (*18, 19*). The N-terminal side of the $(\beta/\alpha)_8$ barrel of the synthase subunit (or domain) was shown to face the active site of the glutaminase subunit (or domain) of an open α/β structure. Interestingly, the synthase and glutaminase active sites are connected by a putative tunnel through the $(\beta/\alpha)_8$ barrel for ammonia transfer with a gate formed by four charged residues at the entrance of the tunnel. On the basis of these structures, the glutaminase activity coupled with the synthase activity and the transfer of ammonia through the tunnel were discussed but are still a matter of investigation.

We have determined the structure of the native IGPs from *Thermus thermophilus* HB8 (*tt*IGPs). The structure of the *tt*IGPs was compared with those of yeast IGPs (yIGPs) and *T. maritima* IGPs (*tm*IGPs), and showed that IGPs may change from an open to closed conformation upon glutamine binding coupled with the PRFAR binding, providing a putative mechanism for the entry of ammonia into the tunnel though the gate. We now report an X-ray crystallographic study of native *tt*IGPs at 2.3 Å resolution.

MATERIALS AND METHODS

Protein Expression, Purification, and Crystallization—The *Nde*I site was built into the plasmid pUC119 at the initiation codon ATG of the lacZ gene by site-directed mutagenesis. The PCR-cloned structural gene of *hisH* or *hisF* from *T. thermophilus* HB8 was inserted between the *Eco*RI and *Nde*I restriction sites of the mutated pUC119. *Escherichia coli* HB101 was transferred with the resultant plasmid, pUC119-*hisF* or pUC119-*hisH*. Both proteins were overexpressed in separate cells. The *tt*IGPS (*hisH/hisF*) was purified by a three-step column chromatography procedure after both cells were mixed in a 1:1 ratio by weight and homogenized by sonication; first on a DEAE-Toyopearl column (Tosoh) equilibrated with buffer A (50 mM KH_2PO_4, pH 7.0, 5 mM β-mercaptoethanol) and washed with 1 liter of buffer A, then a Phenyl-Toyopearl column (Tosoh) equilibrated with buffer B (10 mM KH_2PO_4, pH 7.0, 20% saturated ammonium sulfate, 5 mM β-mercaptoethanol) and eluted with a linear gradient from 20 to 0% saturated ammonium sulfate, and finally on a gigapite column (Seikagaku Kogyo) equilibrated with buffer C (2 mM KH_2PO_4, pH 7.0, 5 mM β-mercaptoethanol) and eluted with a linear gradient of potassium phosphate (2–300 mM).

Crystallization and Data Collection—Crystals of *tt*IGPS (*hisH/hisF*) were obtained by the hanging-drop vapor diffusion method at 293 K (*20*). A 3 μl aliquot of protein solution (5 mg/ml protein, 10 mM Na-HEPES) was mixed with an equal volume of reservoir solution (4.4 M NaCl, 0.1 M Na-HEPES, pH 7.5). After two weeks, crystals had grown to full size (0.3 × 0.3 × 0.2 mm) in the space group $P4_32_12$ with unit cell parameters $a = b = 82.2$, $c = 156.2$ Å. The unit cell volume is consistent with the presence of one heterodimer per asymmetric unit corresponding to a specific volume V_m = 2.70 Å^3/Da and solvent content of 54%. X-ray diffraction experiments on the crystals showed a diffraction up to 2.3 Å resolution at 290 K using a Rigaku RaxisIV++. The data set for the crystals soaked in 1 mM $HgCl_2$ and EMTS was collected to 3.0 Å and 2.9 Å at 293 K using a Rigaku Raxis II c. The native data were processed and scaled using the program Crystal Clear (Molecular Structure Corporation, a Rigaku company) and MIR data were processed and scaled using the programs DENZO and SCALEPACK (*21*).

Structure Determination and Refinement—The structure of *tt*IGPs was solved by the MIR method using two isomorphous data sets. The scaling of all data and map calculations were performed with the CCP4 program suite (*22*). The location of the initial heavy atom sites was determined by the difference Patterson method, and refined by the program SOLVE (*23*). The resulting MIR map has a mean figure of merit of 0.53. The map was improved by the process of solvent flattening with the program RESOLVE (*23*) to give a mean figure of merit of 0.70. The model of *tt*IGPs was gradually built into a 3.0 Å map using the program O (*24*) and a series of refinements were done with the program CNS (*25*). The resolution was increased to 2.3 Å resolution, and several rounds of refinement and manual rebuilding reduced R_{factor} and R_{free} to 24.2 and 29.2%, respectively. Water molecules were picked up on the basis of peak

TABLE I. **Data collection, MIR, and refinement statistics.**

	Native	$HgCl_2$	EMTS[e]
Diffraction data			
Wavelength, Å	1.5418	1.5418	1.5418
Resolution, Å	2.3	3.0	2.9
Total no. of reflections	88,635	51,723	57,811
Unique no. of reflections	23,969	10,900	12,232
Completeness, %	98.8 (99.9)[d]	96.2 (97.3)	97.4 (97.5)
R_{merge} (final shell), %[a]	6.3 (26.1)[d]	8.6 (20.9)	7.5 (22.6)
MIR			
R_{diff}, %[b]		18.8	13.0
phasing power[c]		1.32	1.19
no. of site		2	1
Refinement			
Resolution limits, Å	10–2.3		
R_{factor}, %	20.3		
R_{free}, %	25.6		
Deviations			
Bond length, Å	0.007		
Bond angles, deg	1.4		
Mean *B* factors			
main chain atoms, Å^2	34.66		
side-chain atoms, Å^2	36.01		
water atoms, Å^2	40.90		

[a] $R_{merge} = \sum_{hkl} \sum_i |I_{hkl,i} - \langle I_{hkl} \rangle| / \sum_{hkl} \sum_i I_{hkl,i}$, where I = observed intensity and $\langle I \rangle$ = average intensity for multiple measurements. [b] $R_{diff} = \sum_i^n |F_{PHi}| - |F_P| / \sum_i |F_P|$, where $|F_{PH}|$ and $|F_P|$ are the derivative and native structure-factor amplitudes, respectively. [c] Phasing power is the ratio of the root-mean-square (rms) of the heavy atom scattering amplitude and the lack of closure error. [d] The values in parentheses are for the highest resolution shells (2.38–2.30 Å) in the native enzyme. [e] Ethylmercurithiosalicylic acid, sodium salt.

height and distance criteria from the difference map. Water molecules whose thermal factors were above 65 Å^2 (maximum thermal factor of the main chain) after refinement were removed from the list. Further model building and refinement cycles resulted in an R_{factor} of 20.3% and R_{free} of 25.6%, using 23969 reflections [$F_o > 2\sigma(F_o)$] between 10.0 and 2.3 Å resolution (Table I). The maximum thermal factor of the water molecules was 64.9 Å^2.

Quality of the Structure—The refined model comprises 251 residues for the synthase subunit, 195 residues for the glutaminase subunit, and 118 water molecules. No interpretable electron density was observed for one N-terminal residue (Met1s) of the synthase subunit, and two N-terminal (Met1g and Arg2g) and three C-terminal residues (Glu198g, Val199g, and Leu200g) of the glutaminase subunit. The average and maximum thermal factors of the main chain atoms in the synthase and glutaminase subunits are 63.5 and 65.6 Å^2, respectively.

An analysis of the stereochemistry with PROCHECK (*26*) showed that all main chain atoms (except for Cys 82 in the glutaminase subunit) fall within the generously allowed region of the Ramachandran plot with 331 residues in the most favored region and 36 in the additionally allowed region. Structure diagrams were drawn using the programs Molscript (*27*), Bobscript (*28*), and Raster3D (*29*).

RESULTS AND DISCUSSION

Description of the Structure—The overall structure of *tt*IGPs is shown in Fig. 1. The *tt*IGPs consists of glutaminase and synthase subunits. The glutaminase subunit is folded into an open α/β structure similar to those of the glutaminase subunits in class I glutamine-dependent amidotransferases (*4–9*). The glutaminase subunit predominantly consists of β-strands, and is characterized by an open β-sheet of seven strands (b1g, b2g, b3g, b4g, b9g, b10g, and b11g) that are all parallel except for b10g. One side of the large β-sheet as the central core is covered by α-helices, a1g and a4g, and an antiparallel β-sheet of two strands (b7g and b8g), and the other side by α-helices a2g and a2′g, and a three-stranded β-sheet of b5g, b6g, and b8′g.

The synthase subunit has a typical β/α barrel structure comprising eight β-strands and α-helices (Fig. 2) (*30*). The large and deep crevice for binding the substrate PRFAR is formed on the C-terminal side of the barrel, which has long loops connecting the C-terminus of a β-strand and the N-terminus of an α-helix. The side-chains of the β-strands protrude toward the inside of the barrel in four layers. The first layer located at the N-terminal side of the barrel consists of four charged residues, Arg6, Glu47, Lys100, and Glu168, that form a cyclic salt bridge to close the bottom of the barrel. These four residues are completely conserved in *tt*IGPs, *tm*IGPs, and yIGPs. The second and third layers are made up of three bulky hydrophobic residues and one hydrophilic Ser or Thr. The residues Cys10s, Gly81s, Ala129s, and Ser202s form the fourth layer on the C-terminal side of the barrel, leaving a relatively large space inside the barrel. In the center of the barrel is a tunnel through which small molecules such as water or ammonia may go, although the bottom of the barrel is closed by the cyclic salt bridge. The N-terminal side of the $(\beta/\alpha)_8$ barrel of the synthase subunit makes a subunit interface with the loop region of the N-terminal side of the central β-sheet and the two-stranded β-sheet of b7g and b8g of the glutaminase subunit (Figs. 1 and 2).

Comparison of the ttIGPs Structure with Those of tmIGPs and yIGPs—The glutaminase and synthase subuits of *tt*IGPs have sequence identities of 35 and 57% with those of *tm*IGPs, and 30.5 and 35.1% with the glutaminase and synthase domains of yIGPs, respectively. The Cα atoms of the glutaminase subunit in *tt*IGPs can be superimposed onto the corresponding atoms in *tm*IGPs and yIGPs within rms deviations of 0.83 and 0.83 Å with maximum displacements of 1.48 and 1.36 Å, respectively (Fig. 3) (*18, 19*). The corresponding Cα atoms between the synthase subunit in *tt*IGPs, and those in *tm*IGPs and yIGPs fit within 0.66 and 0.83 Å with maximum displacements of 1.46 and 1.51 Å, respectively (Fig. 3). The synthase and glutaminase subunits (domains) of these three IGPs enzymes thus have very similar folding of the main chain except for the elongated loops of the N-terminal side of the β-barrel in the synthase domain of yIGPs.

Although the overall structure of each subunit (domain) is conserved in these enzymes, the relative location of the

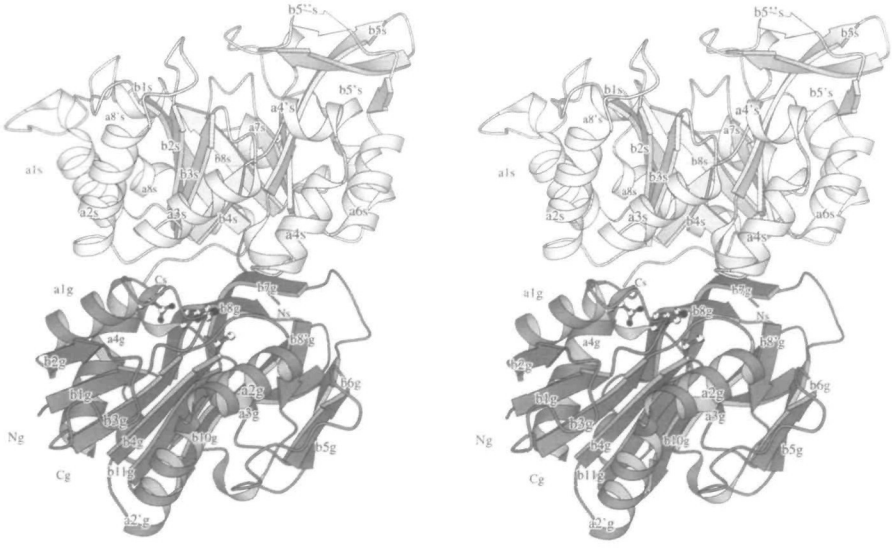

Fig. 1. **Stereoview of the overall structure of *tt*IGPs with secondary structure assignment.** The glutaminase subunit is represented by the heavily shaded ribbon, and the synthase subunit by the lightly shaded ribbon. α-Helices of the glutaminase and synthase subunits are denoted as a1g–a4g and a1s–a8s, respectively, and β-sheets as b1g–b11g and b1s b8s, respectively. The central cavity is the glutaminase site formed between the subunit interface. The catalytic triad (Cys83g, His193g, and Glu193g) for glutamine hydrolysis, and Glu124s, which is from the synthase subunit and recognizes the substrate glutamine, are shown by the ball-and-stick models.

Fig. 2. **The synthase subunit viewed from a pseudo 8-fold axis.** (a) Stereoview of the synthase subunit. The C-terminal side of the barrel has a large and long crevice for binding the substrate PRFAR. The bottom (N-terminal side) of the barrel is closed by the cyclic salt bridge formed by Arg6s, Glu47s, Lys100s, and Glu168s. A two-stranded antiparallel β-sheet (b7g and b8g) of the glutaminase subunit is located just under Arg6s and Glu47g. (b) CPK model of the synthase subunit. The ammonia tunnel is shown in the center of the molecule with the heavily shaded molecular surface.

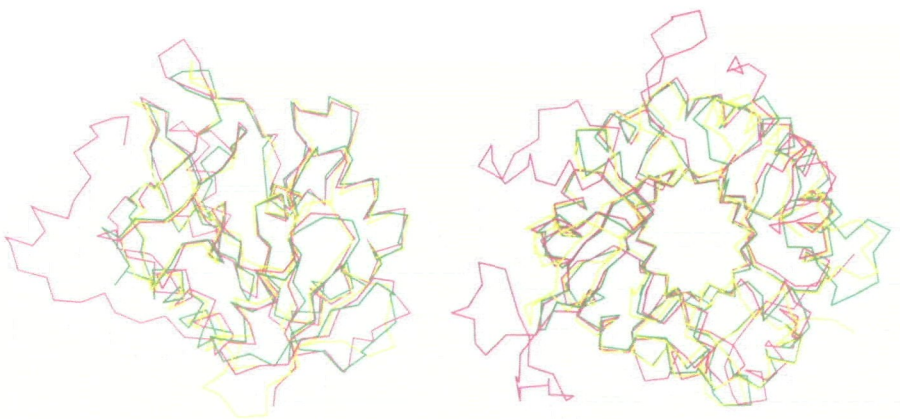

Fig. 3. **Superposition of the glutaminase (left) and synthase (right) subunits of *tt*IGPs, *tm*IGPs, yIGPs by least-squares fitting of Cα-atoms, indicating that the folding of each subunit (domain) is well conserved among these three IGPs except for the elongated loops caused by the insertion of amino acid residues.** The green, yellow, and pink lines represent *tt*IGPs, *tm*IGps, and yIGPs, respectively.

synthase subunit (domain) to the glutaminase subunit (domain) differs from one to another. The superposition of the synthase subunit of *tt*IGPs on that of yIGPs shows a significant deviation of the main chain of the glutaminase subunits (Fig. 4). The superposition of the synthase subunits of *tm*IGPs and yIGPs displays an even larger deviation of the main chain of the glutaminase subunits. These deviations are explained by the change in the relative orientation between the synthase and glutaminase subunits in these enzymes. When compared with the relative orientations observed in *tt*IGPs and *tm*IGPs, yIGPs changes its relative orientation to close the glutamine binding pocket located on the glutaminase side of the subunit interface, resulting in a larger accessible surface area of 3493 Å^2 in yIGPs as compared with 2722 Å^2 in *tt*IGPs and 2303 Å^2 in *tm*IGPS.

The Glutaminase Active Site and Open-Closed Conformational Change—The glutamine binding pocket is formed by Pro47g–Gly50g, Cys82g, Val83g, Gln86g, Glu94g, Ser143g, Tyr144g, His178g, and Glu180g in the glutaminase subunit, and Gln124s in the synthase subunit. These active site residues are completely conserved among *tt*IGPs, *tm*IGPs, and yIGPs. In the case of yIGPs, an inhibitor (acivicin) forms a covalent bond with the catalytic residue Cys82g and interacts with the neighboring residues (*18*). The inhibitor is encapsulated into the active site cavity and isolated from the solvent region (Fig. 5). On the other hand, the glutamine binding pockets of *tt*IGPs and *tm*IGPs in their free form allow access of solvent molecules to the catalytic residue Cys82g.

The *tt*IGPs and yIGPs were superimposed by least-squares fitting of the corresponding Cα atoms of β-barrels in the synthase subunit (Fig. 5). Interestingly, many of the active site residues of *tt*IGPs show large positional deviations from the corresponding residues in yIGPs. These deviations are correlated with the change in the relative orientation between the glutaminase and synthase subunits described above. This change induces active site closure and makes interactions of inhibitor or substrate molecules with the neighboring residues possible. Presumably, free yIGPs, which has an open conformation similar to those observed for *tt*IGPs and *tm*IGPs, changes its relative orientation between the synthase and glutaminase subunits upon inhibitor or substrate binding to close the glutamine binding pocket and sequester it from the solvent (*31*).

Although *tt*IGPs was cocrystallized with the inhibitor acivicin, the acivicin was not bound to the enzyme. This is consistent with the view that IGPs does not show glutami-

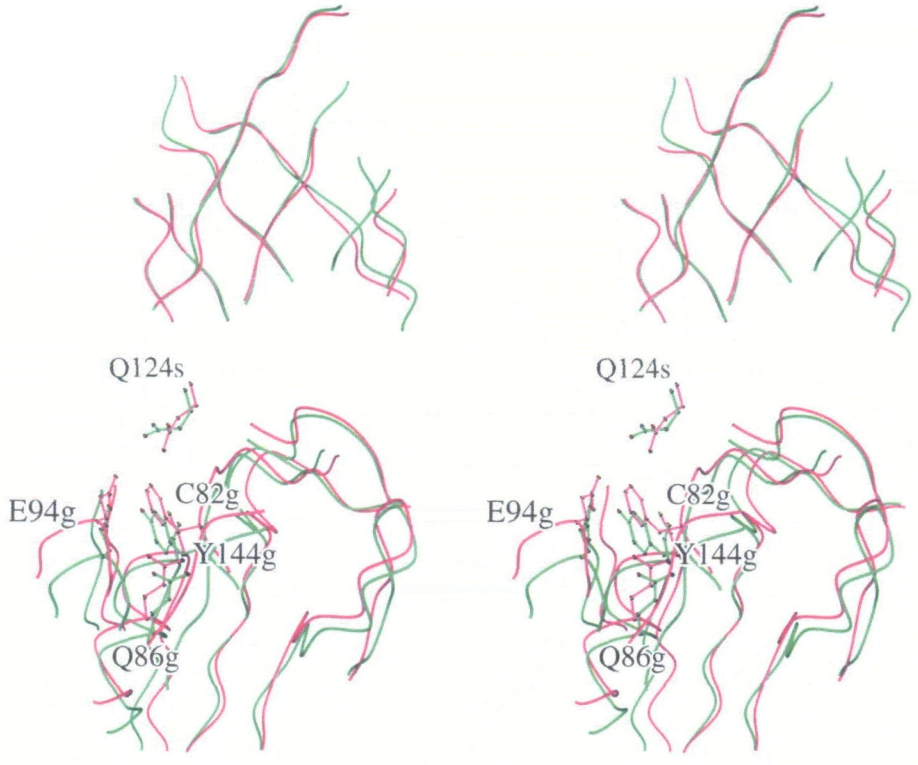

Fig. 4. **Superposition of *tt*IGPs onto yIGPs by least-square fitting of the Cα-atoms of β-barrels in the synthase subunits.** The green and pink lines represent *tt*IGPs and yIGPs, respectively. While the β-barrels show good superposition between *tt*IGPs and yIGPs, the main-chain of the glutaminase subunit in yIGPs deviates from the corresponding chain in *tt*IGPs with marked shifts around the glutaminase site. C82g is the catalytic residue in the glutaminase subunit, and Q124s in the synthase subunit is supposed to interact with the substrate glutamine (q). Q86g, E94g, and F144g of yIGPs are located close to the glutaminase site in comparison with the corresponding residues in *tt*IGPs.

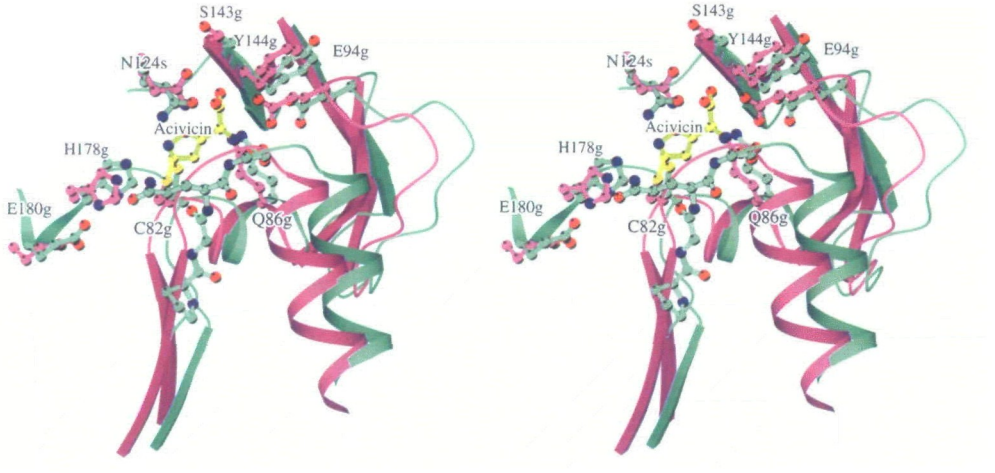

Fig. 5. **Superposition of the active-site regions between *tt*IGPs (green) and yIGPs (purple) by least-squares fitting of the Cα atoms of β-barrels in the synthase subunits.** The amino acid residues of the glutaminase site and the inhibitor (acivicin) bound to yIGPs are shown. The residues of yIGPS move to close the active-site cavity and interact with the inhibitor, while the active site of *tt*IGPs is in an open conformation.

nase activity in the absence of substrate (PRFAR). The cocrystallization of yIGPs with the acivicin in the presence of PRFAR gave a complex crystal with acivicin covalently bound to the enzyme (*18*). The glutaminase activity of yIGPs coupled with PRFAR binding to the synthase site induced a conformational change in IGPs to activate the glutaminase site and bind acivicin. The closed form observed in the yIGPS complex with acivicin may be different in some degree from the true active form of the enzyme, since the synthase subunit has a structure similar to that of *tt*IGPs or *tm*IGPs, and does not bind PRFAR. However, the yIGPs complex in which acivicin is encapsulated in the glutaminase site is in a favorable conformation for Gln124s of the synthase subunit to interact with the substrate glutamine and to prevent nascent ammonia from diffusing to the solvent side. Thus, the open-closed conformational change in IGPs enzymes may play an important role in the glutaminase activity coupled with the synthase reaction.

Implication for Ammonia Transfer through the Molecular Tunnel of the Barrel—On the basis of the X-ray structures of yIGPs and *tm*IGPs, it was reasonably assumed that the nascent ammonia produced at the glutaminase activity site enters the tunnel of the barrel, and reaches the synthase site to react with PRFAR (*18, 19*). The remaining problem to be solved is the mechanism by which ammonia passes through the cyclic salt bridge formed by the four charged residues at the subunit interface.

Out of the four charged residues of the salt bridge, the side chains of Arg6s, Glu47s, and Asp168s are covered by hydrophobic side chains of the β-sheet comprising b7g and

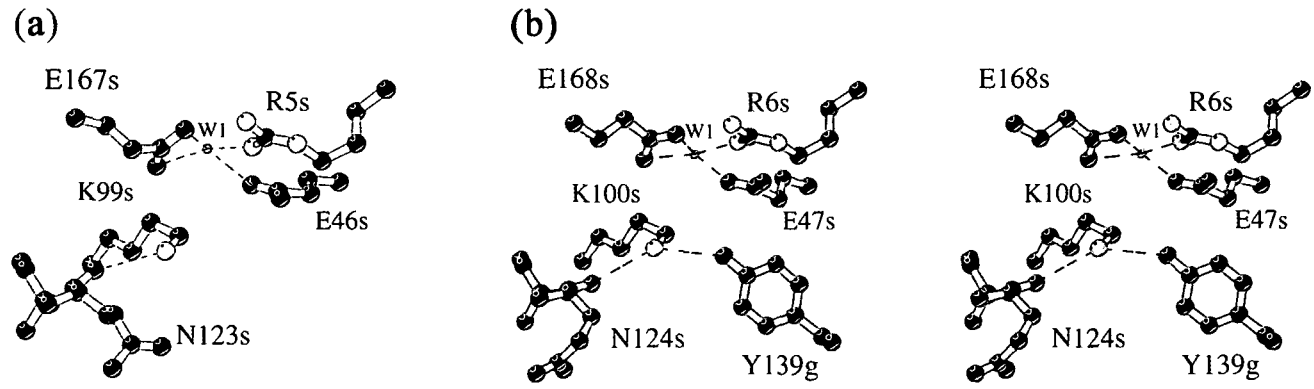

Fig. 6. **The side-chain movement of Lys100s to open the cyclic salt bridge.** (a) K99s (K100s in ttIGPs) is observed to be free from the cyclic salt bridge and to make a hydrogen bond with N123s (N124s in ttIGPs) in the isolated synthase subunit of *tm*IGPs. A water molecule (W1) interacts with three charged residues of the salt bridge. (b) The arrangement of K99s and the water molecule (W1) shown in (a) are copied into the *tt*IGPs structure giving an ammonia tunneling model. Hydrogen bond distances between the water molecule and charged residues are in the range from 2.6 to 3.2 Å.

b8g of the glutaminase subunit, resulting in a restriction of the conformational flexibility of these residues, and the strengthening of the salt bridges between Arg6s, and Glu47s and Asp168s. On the other hand, Lys100s of the salt bridge is located just above the hydrophilic cavity of the glutaminase site, and has space to make a conformational change in its side chain possible. The mobility of the side chain of Ly100s is supported by the X-ray structure of *tm*IGPs in which the salt bridges between Lys100s and Glu167s are elongated to 4.1 and 4.5 Å in two of the three independent molecules in the asymmetric unit (*19*). Moreover, Lys100s is neighbored by Tyr139g of the glutaminase subunit in *tt*IGPs, yIGPs, and *tm*IGPs with the formation of a direct hydrogen bond in *tt*IGPs. This interaction has been pointed out to play an important role in loosening the salt bridge around Lys100s (*18*). Lys100s is thus the most plausible candidate for the door to the ammonia tunnel.

IGPs or isolated synthase subunits have synthase activity in the presence of ammonium salt (*15, 16*), suggesting that the passage of ammonia through the cyclic salt bridge is not correlated with the glutaminase activity. Ammonium ions in solution may enter the ammonia tunnel in the same manner as nascent ammonia from the hydrolysis of glutamine, although the ammonium ion must be deprotonated. The possible conformational change of Lys100s to open the cyclic salt bridge is observed in the X-ray structure of the isolated synthase subunit of *tm*IGPs (*17*). The amino group of Ly100s is disordered into two positions in this synthase structure (Fig. 6a). One of two disordered amino groups loses the salt bridge with Glu47s to form a hydrogen bond with the main chain carbonyl group of Gln124s, indicating that the side chain of Lys100s may change its direction and make a small opening to the ammonia tunnel. A water molecule is located at the center of the salt bridge and interacts with the charged side-chains of Arg6s, Glu47s, and Glu168s. The local structure around this salt bridge is modeled into the *tt*IGPS complex structure (Fig. 6b). In addition to Gln123s, Tyr139g forms a hydrogen bond with Lys100s, suggesting that residues from both subunits cooperate to loosen the salt bridge with Lys100s. If the water molecule that interacts with Arg6s, Glu47s, and Glu168s is replaced by an ammonia molecule, the model structure seems to mimic ammonia tunneling. Lys100s might change its side chain conformation toward Gln124s and Tyr139g to make space for ammonia to enter into the tunnel of the synthase barrel.

REFERENCES

1. Zalkin, H. (1993) The amidotransferases. *Adv. Enzymol. Relat. Areas Mol. Biol.* **66**, 203–309
2. Zalkin, H. and Smith, J.L. (1998) Enzymes utilizing glutamine as an amide donor. *Adv. Enzymol. Relat. Areas Mol. Biol.* **72**, 87–144
3. Massiere, F. and Badet-Denisot, M.A. (1998) The mechanism of glutamine-dependent amidotransferases. *Cell. Mol. Life Sci.* **54**, 205–222
4. Knochel, T., Ivens, A., Hester, G., Gonzalez, A., Bauerle, R., Wilmanns, M., Kirschner, K., and Jansonius, J.N. (1999) The crystal structure of anthranilate synthase from *Sulfolobus solfataricus*: functional implications. *Proc. Natl. Acad. Sci. USA* **96**, 9479–9484
5. Spraggon, G., Kim, C., Nguyen-Huu, X., Yee, M.C., Yanofsky, C., and Mills, S.E. (2001) The structures of anthranilate synthase of *Serratia marcescens* crystallized in the presence of (i) its substrates, chorismate and glutamine, and a product, glutamate, and (ii) its end-product inhibitor, L-tryptophan. *Proc. Natl. Acad. Sci. USA* **98**, 6021–6026
6. Thoden, J.B., Holden, H.M., Wesenberg, G., Raushel, F.M., and Rayment, I. (1997) Structure of carbamoyl phosphate synthetase: a journey of 96 Å from substrate to product. *Biochemistry* **36**, 6305–6316
7. Thoden, J.B., Miran, S.G., Phillips, J.C., Howard, A.J., Raushel, F.M., and Holden, H.M. (1998) Carbamoyl phosphate synthetase: caught in the act of glutamine hydrolysis. *Biochemistry* **37**, 8825–8831
8. Thoden, J.B., Huang, X., Raushel, F.M., and Holden, H.M. (1999) The small subunit of carbamoyl phosphate synthetase: snapshots along the reaction pathway. *Biochemistry* **38**, 16158–16166
9. Parsons, J.F., Jensen, P.Y., Pachikara, A.S., Howard, A.J., Eisenstein, E., and Ladner, J.E. (2002) Structure of *Escherichia coli* aminodeoxychorismate synthase: architectural conservation and diversity in chorismate-utilizing enzymes. *Biochemistry* **41**, 2198–2208
10. Hyde, C.C., Ahmed, S.A., Padlan, E.A., Miles, E.W., and Davies, D.R. (1988) Three-dimensional structure of the tryptophan synthase $\alpha_2\beta_2$ multienzyme complex from *Salmonella typhimurium*. *J. Biol. Chem.* **263**, 17857–17871
11. Rhee, S., Miles, E.W., and Davies, D.R. (1998) Cryo-crystallography of a true substrate, indole-3-glycerol phosphate, bound to

a mutant (αD60N) tryptophan synthase $\alpha_2\beta_2$ complex reveals the correct orientation of active site αGlu49. *J. Biol. Chem.* **273**, 8553–8555
12. Weyand, M. and Schlichting, I. (1999) Crystal structure of wild-type tryptophan synthase complexed with the natural substrate indole-3-glycerol phosphate. *Biochemistry* **38**, 16469–16480
13. Alifano, P., Fani, R., Lio, P., Lazcano, A., Bazzicalupo, M., Carlomagno, M.S., and Bruni, C.B. (1996) Histidine biosynthetic pathway and genes: structure, regulation, and evolution. *Microbiol. Rev.* **60**, 44–69
14. Chittur, S.V., Chen, Y., and Davisson, V.J. (2000) Expression and purification of imidazole glycerol phosphate synthase from *Saccharomyces cerevisiae*. *Protein Expr. Purif.* **18**, 366–377
15. Klem, T.J. and Davisson, V.J. (1993) Imidazole glycerol phosphate synthase: the glutamine amidotransferase in histidine biosynthesis. *Biochemistry* **32**, 5177–5186
16. Beismann-Driemeyer, S., and Sterner, R. (2001) Imidazole glycerol phosphate synthase from *Thermotoga maritima*. Quaternary structure, steady-state kinetics, and reaction mechanism of the bienzyme complex. *J. Biol. Chem.* **276**, 20387–20396
17. Lang, D., Thoma, R., Henn-Sax, M., Sterner, R., and Wilmanns, M. (2000) Structural evidence for evolution of the β/α barrel scaffold by gene duplication and fusion. *Science* **289**, 1546–1550
18. Chaudhuri, B.N., Lange, S.C., Myers, R.S., Chittur, S.V., Davisson, V.J., and Smith, J.L. (2001) Crystal structure of imidazole glycerol phosphate synthase: a tunnel through a $(\beta/\alpha)_8$ barrel joins two active sites. *Structure* **9**, 987–997
19. Douangamath, A., Walker, M., Beismann-Driemeyer, S., Vega-Fernandez, M.C., Sterner, R., and Wilmanns, M. (2002) Structural evidence for ammonia tunneling across the $(\beta\alpha)_8$ barrel of the imidazole glycerol phosphate synthase bienzyme complex. *Structure* **10**, 185–193
20. Jancarik, J. and Kim, S.-H. (1991) Sparse matrix sampling: a screening method for crystallization of proteins. *J. Appl. Crystallogr.* **24**, 409–411
21. Otwinowski, Z. (1993) Data collection and processing in *Proceedings of the CCP4 Study Weekend*, pp. 56–62, SERC Daresbury Laboratory, Warrington
22. Collaborative Computational Project Number 4 (1994) The CCP4 suite: programs for protein crystallography. *Acta Crystallogr.* **D50**, 760–763
23. Terwilliger, T.C. and Berendzen, J. (1999) Automated MAD and MIR structure solution. *Acta Crystallogr.* **D55**, 849–861
24. Jones, T.A., Zou, J.-Y., Cowan, S.W., and Kjeldgaard, M. (1991) Improved methods for building protein models in electron density maps and the location errors in these models. *Acta Crystallogr.* **A47**, 110–119
25. Brunger, A.T., Adams, P.D., Clore, G.M., DeLano, W.N., Gros, P., Grosse-Kunstleve, R.W., Jiang, J.-S., Kuszewski, J., Nilges, M., Pannu, N.S., Read, R.J., Rice, L.M., Simonson, T., and Warren, G.L. (1998) Crystallography & NMR system: A new software suite for macromolecular structure determination. *Acta Crystallogr.* **D54**, 905–921
26. Laskowski, R.A., MacArthur, M.W., Moss, D.S., and Thornton, J.M. (1993) PROCHECK: a program to check the stereochemical quality of protein structures. *J. Appl. Crystallogr.* **26**, 283–291
27. Kraulis, P.J. (1991) MOLSCRIPT: a program to produce both detailed and schematic plots of protein structures. *J. Appl. Crystallogr.* **24**, 946–950
28. Esnouf, R.M. (1997) An extensively modified version of Molscript that includes greatly enhanced coloring capabilities. *J. Mol. Graph. Model.* **15**, 132–134
29. Merritt, E.A. and Murphy, M.E.P. (1994) Raster3D version 2.0: a program for photorealistic molecular graphics. *Acta Crystallogr.* **D50**, 869–873
30. Hocker B., Jurgens C., Wilmanns M., and Sterner R. (2001) Stability, catalytic versatility and evolution of the $(\beta\alpha)_8$-barrel fold. *Curr. Opin. Biotechnol.* **12**, 376–381
31. Gerstein M., Lesk A.M., and Chothia C. (1994) Structural mechanisms for domain movements in proteins. *Biochemistry* **33**, 6739–6749